On the Use of Entire-Domain Basis Functions in Galerkin Methods Applied to Certain Integral Equations for Wire Antennas With the Approximate Kernel

George Fikioris and Asimina Michalopoulou

***Abstract*—When the approximate kernel is used, Hallén's integral equation for the current distribution on a center-driven, straight-wire antenna does not have a solution. This is true for at least two types of feed: the delta-function generator and the frill generator. For the case of subsectional basis functions in Galerkin's method, recent papers have shown that the main associated difficulty is the unavoidable appearance of oscillations near the center and/or the ends of the antenna. In this paper, we investigate the nature of the difficulties for the case of entire-domain, cosine basis functions. We find that the difficulties are similar to those of the subsectional case, something that we had not expected beforehand. In particular, undesirable oscillations appear when the number of basis functions is greater than a number dependent on the length-to-radius ratio, giving one a simple rule for choosing the number of basis functions so as to yield smooth solutions. We also compare results to "true" solutions, study the separate but important effects of roundoff, and give extensions to equations of the Pocklington type.**

***Index Terms*—Antenna feeds, antenna theory, Galerkin method, integral equations, wire antennas.**

I. Introduction

The accurate determination of currents on wire antennas has been a fundamental electromagnetic compatibility (EMC) problem for many years [1]–[5]. The preferred method of approach is the solution of integral equations of the Hallén or Pocklington type, which apply to a variety of EMC-related wire antenna problems [6]–[9]. In the present paper, we discuss Hallén's equation (HE) and Pocklington's equation (PE) for the simple case of the straight, center-driven wire of length $2h$. The unknown is the current $I(z)$, and HE and PE are to be solved together with the condition $I(\pm h) = 0$.

The aforementioned equations are used with (at least) two types of feed, the delta-function generator (DFG) and the frill generator (FG) (we specifically refer to the "magnetic FG" discussed in [10] and [11]), and two types of kernel, the exact and the approximate (or reduced) kernel. Although a number of recent papers [3], [12]–[14] describe accurate and efficient methods of using the more complicated exact kernel, the simpler approximate kernel is used in standard modern antenna and EMC textbooks [4], [10], [15], standard antenna analysis software such as the Numerical Electromagnetics Code (NEC) [16], not to mention a large number of recent research papers. Thus, although the approximate kernel often gives good results, it is important to thoroughly understand the difficulties associated with its use.

With the approximate kernel, it has been pointed out [12], [17], [18] that the integral equations are ill-posed. Furthermore, for HE, and in both the DFG and the FG cases, it has been shown in [19] (also see [20]) and [11] that the corresponding equations—(1) and (7)—have no solutions, something not mentioned in many recent textbooks.

Manuscript received May 7, 2007; revised October 22, 2008. First published March 21, 2009; current version published May 15, 2009. The work of G. Fikioris was supported by the Leykippos Basic Research Program.

G. Fikioris is with the School of Electrical and Computer Engineering, National Technical University of Athens, GR 157-73 Zografou, Greece (e-mail: gfiki@cc.ece.ntua.gr).

A. Michalopoulou is with the School of Electrical and Computer Engineering, National Technical University of Athens, GR 157-73 Zografou, Greece, and also with the Mobile Communications Laboratory, Institute of Informatics and Telecommunications, National Center of Scientific Research "Demokritos," Athens GR 153-10, Greece (e-mail: asimihal@esd.ntua.gr).

Digital Object Identifier 10.1109/TEMC.2008.2010711

In this paper, we examine consequences associated with the aforementioned mathematical properties for the case where a sufficiently large number of entire-domain basis functions is used in Galerkin's method. We specifically consider cosines for HE and cosines that vanish at $z = \pm h$ for PE, but we believe that our conclusions carry over to other entire-domain basis functions. The present paper supplements [11] and [21], which, for the case of *subsectional* basis functions, show that the main consequence is the appearance of rapid oscillations near $z = \pm h$. For the DFG case [21], but not for the FG case [11], there are also oscillations near the driving point $z = 0$.

Here, perhaps surprisingly, we find oscillating effects quite similar to the case of subsectional basis functions, and indicate how to recognize and avoid them. We stress that the aforementioned oscillating effects are not due to roundoff errors, and we discuss the latter effects separately. The distinction is important because effects due to roundoff can possibly be avoided by using computers with longer word lengths, but the aforementioned oscillating effects occur even for arbitrarily large word lengths and cannot be avoided by more powerful computers. As in [11] and [21], and as long as the approximate kernel is used, we believe that many of our conclusions carry over to integral equations for more complicated types of antennas (e.g., arrays of wire antennas, curved-wire antennas).

An $e^{-i\omega t}$ time dependence is assumed, where $\omega = kc = 2\pi c/\lambda$. V denotes the driving voltage, a the wire radius, b is the outer radius of the FG, and $\zeta_0 = 376.73\ \Omega$. Some of the results herein have been presented previously in [22].

II. Hallén's Equation

HE is [11, eq. (3)], [21, eq. (1)]

$$\int_{-h}^{h} K(z-z')I(z')\,dz' = f_1(z) + C\,\cos kz, \quad -h < z < h \tag{1}$$

where

$$K(z) = \frac{1}{4\pi}\frac{\exp\left(ik\sqrt{z^2+a^2}\right)}{\sqrt{z^2+a^2}} \tag{2}$$

is the approximate kernel, C is a constant to be determined from $I(\pm h) = 0$, and

$$f_1(z) = \begin{cases} iV(2\zeta_0)^{-1}\sin k|z|, & \text{DFG case} \\ k^{-1}\int_0^z g(t)\sin k(z-t)\,dt, & \text{FG case} \end{cases} \tag{3}$$

$$g(z) = \frac{ikV}{2\zeta_0\,\ln(b/a)}\left[\frac{\exp\left(ik\sqrt{z^2+a^2}\right)}{\sqrt{z^2+a^2}} - \frac{\exp\left(ik\sqrt{z^2+b^2}\right)}{\sqrt{z^2+b^2}}\right]. \tag{4}$$

For the two feeds considered here, HE does not have a solution: to be precise, for the DFG case, (1) can admit no solution $I(z)$ belonging to $L^1(-h,h)$ [19], while for the FG case, (1) can admit no continuous solution $I(z)$ [11].

For either generator, our numerical method consists of writing $I(z) = I^{(1)}(z) + CI^{(2)}(z)$, where $I^{(1)}(z)$ satisfies (1) with the right-hand side (RHS) of (1) replaced by $f_1(z)$, while $I^{(2)}(z)$ satisfies (1) with its RHS replaced by $\cos kz$. We then solve for $I^{(1)}(z)$ and $I^{(2)}(z)$ using Galerkin's method with basis functions $\cos(n\pi z/h)$, $n = 0, 1, \ldots, N$. This leads to two $(N+1)\times(N+1)$ systems of equations for the basis function coefficients $I_n^{(1)}$ and $I_n^{(2)}$. Once the two systems are solved, we determine C from

$$C \cong -\frac{\sum_{n=0}^{N}(-1)^n I_n^{(1)}}{\sum_{n=0}^{N}(-1)^n I_n^{(2)}} \tag{5}$$

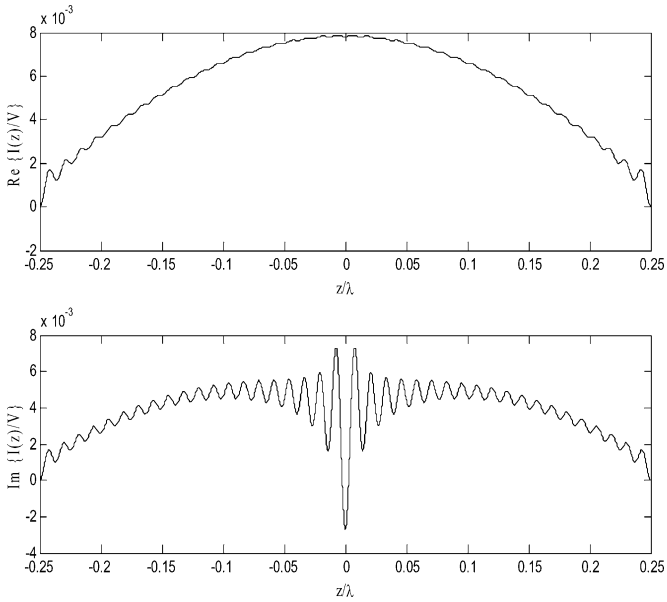

Fig. 1. (Top) Re$\{I(z)/V\}$ and (bottom) Im$\{I(z)/V\}$ as calculated by the numerical method of Section II (in amperes per volt). HE/DFG combination; $h/\lambda = 0.25$, $a/\lambda = 0.01$, and $N = 40$. The value at $z = 0$ is $I(0)/V = (7.8 - j2.7)$ mS.

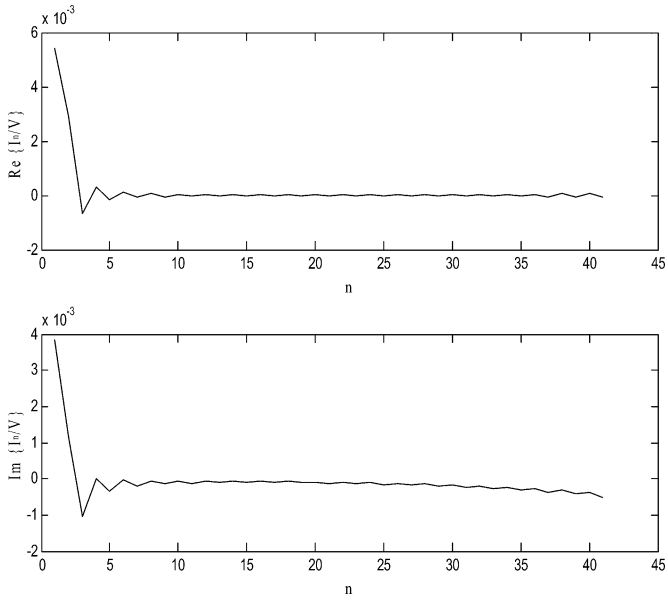

Fig. 2. Basis function coefficients (top) Re$\{I_n/V\}$ and (bottom) Im$\{I_n/V\}$ as calculated by the numerical method of Section II (in amperes per volt). HE/DFG combination; $h/\lambda = 0.25$, $a/\lambda = 0.01$, and $N = 40$.

and the final approximate solution that vanishes at $z = \pm h$ is

$$I(z) \cong \sum_{n=0}^{N} I_n \cos\left(\frac{n\pi z}{h}\right) = \sum_{n=0}^{N} \left[I_n^{(1)} + C I_n^{(2)}\right] \cos\left(\frac{n\pi z}{h}\right). \tag{6}$$

Fig. 1 shows $I(z)/V$ for the DFG case with $N = 40$, $h/\lambda = 0.25$, and $a/\lambda = 0.01$, so that $h/a = 25$. The most striking abnormal behavior is the appearance of rapid oscillations in the imaginary part. These oscillations occur everywhere along the antenna and their amplitudes increase as one moves toward $z = 0$, where the DFG is located. The real part also oscillates, but the amplitudes are smaller and increase near the endpoints $z = \pm h$. Both Re$\{I(z)\}$ and Im$\{I(z)\}$ behave in a manner not dissimilar to the case where subdomain basis functions are used; compare Fig. 1 to [21, Figs. 1 and 2]: the effects of the DFG are more pronounced in its immediate vicinity, and so are the effects of the endpoints. Also, oscillations near the DFG occur only in the imaginary part.

If (1) were a solvable integral equation, then I_n would approach zero for increasing n (for sufficiently large N, at least), which is not the case: as seen in Fig. 2, Re$\{I_n/V\}$ appear to oscillate about zero, whereas Im$\{I_n/V\}$ eventually grow in magnitude. The behavior of Re$\{I_n/V\}$ is associated with the oscillations near $z = \pm h$ in Re$\{I(z)/V\}$, whereas the behavior of Im$\{I_n/V\}$ is associated with the more abnormal oscillations near $z = 0$ in Im$\{I(z)/V\}$.

By varying h/λ, a/λ, and N, we found that the point n after which the Im$\{I_n/V\}$ grow depends on the important parameter h/a, not on h/λ or a/λ separately. In fact, we roughly estimated n to be around $0.6h/a$ (=15 in Figs. 1 and 2), and N must be chosen smaller than this to avoid oscillations. For sufficiently large h/a, this always leads to smooth solutions. As has been pointed out in a slightly different context [11], however, such a "flexibility" in choosing N still does not help determine the *optimal* value of N.

Fig. 3 is similar to Fig. 1, but for the FG. As with subdomain basis functions [11], no oscillations occur near $z = 0$. This can be explained by the analytical study [11] of the antenna of infinite length, which

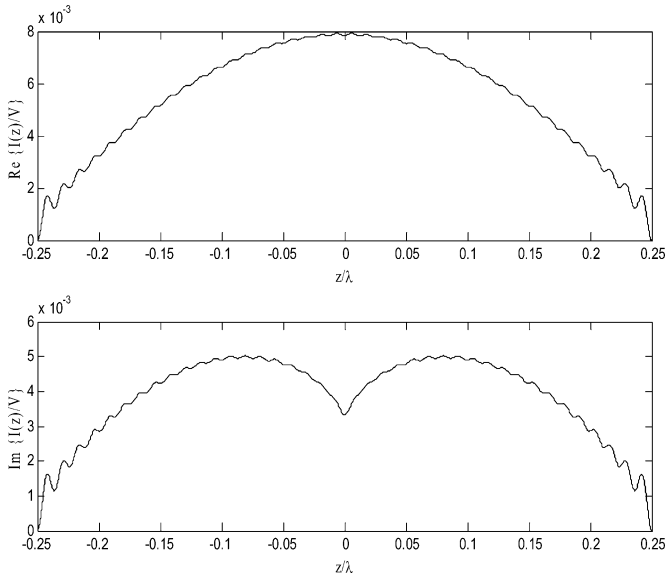

Fig. 3. Same as Fig. 1 but with the FG with $b/a = 2.3$ instead of the DFG. The value at $z = 0$ is $I(0)/V = (7.9 + j3.4)$ mS.

is governed by a solvable integral equation, so that no oscillations occur [11]. Thus, when the length is finite, one should not expect oscillations near the FG. Here, for large n, the Im$\{I_n/V\}$ oscillate about zero, as in Fig. 2 (top).

It is of interest to compare our results to "true" values. We obtained such values for $I(0)/V = G + jB$ by applying the method of [11] and [21]—i.e., Galerkin's method with pulse functions—to HE with the *exact* kernel. Let us denote the number of pulse functions by $2N_p + 1$. For G in the DFG case and for *both* G and B in the FG case, true values (corresponding to $N_p = \infty$) can be obtained using moderate N_p in conjunction with the convergence acceleration methods of [14]. We thus obtained $G = 8.3$ mS for *both* the DFG and the FG cases, which is quite close to the values 7.8 and 7.9 mS in Figs. 1 and 3,

respectively. For the FG case, we found $B = 3.6$ mS, which is quite close to the value 3.4 mS of Fig. 3. For the DFG case, it is not possible to obtain a value B corresponding to $N_p = \infty$ because $\mathrm{Im}\{I(z)/V\}$ is logarithmically singular at $z = 0$ [19], [21]. One way to make a meaningful comparison is to choose $N_p = 40$, so that the two systems of equations in each method have the same size (41×41): we thus obtained $B = 2.1$ mS, which is of the same order of magnitude as the "mean" of the oscillating values near $z = 0$ in Fig. 1 (bottom).

III. Extensions to PE

PE [11, eq. (2)], [21, eq. (42)] results from applying $\mathcal{L} = \partial^2/\partial z^2 + k^2$ to (1). For the FG case, it is shown in [11] that PE can admit no continuous solution $I(z)$. For the DFG case, the authors still consider that PE has no solution[1]; but a precise statement of nonsolvability is beyond the scope of this paper.

Here, we pass $\mathcal{L}$ inside the integral in (1), perform the resulting differentiations as in [10], and end up with a slightly different form than [11, eq. (2)] and [21, eq. (42)]. It is

$$\int_{-h}^{h} G(z-z')I(z')\,dz' = f_2(z), \qquad -h < z < h \tag{7}$$

$$G(z) = \frac{1}{4\pi}\frac{\exp(ikR)}{R^5}\left[k^2a^2R^2 + (1-ikR)(2R^2-3a^2)\right]$$

$$R = \sqrt{z^2+a^2} \tag{8}$$

$$f_2(z) = \begin{cases} iVk\zeta_0^{-1}\,\delta(z), & \text{DFG case} \\ g(z), & \text{FG case} \end{cases} \tag{9}$$

in which $g(z)$ was defined in (4). For the FG case, it is readily checked that the nonsolvability arguments of [11] still hold for the form of PE in (7). Thus, in the FG case, (7)—just like [11, eq. (2)]—has no continuous solution.

We solve (7) numerically by directly applying Galerkin's method with basis functions $\cos[(2n-1)\pi z/(2h)]$, $n = 1, 2, \ldots, N+1$. We found very similar results, i.e., for large N, we always found oscillations near $z = \pm h$ (in both the real and the imaginary parts, and for both the DFG and the FG). In the DFG case, we found additional oscillations near $z = 0$ in the imaginary part, but no such oscillations in the real part. In particular, with h/λ, a/λ, and N as in Fig. 1, we obtained very similar (but not identical) curves.

IV. Condition Numbers

We now turn to important effects separate from those shown in Figs. 1–3. Fig. 4 shows the logarithm (to base 10) of the condition numbers c of the $(N+1) \times (N+1)$ systems of Sections II and III. Fig. 4 (which can be compared to [11, Fig. 3]) shows the following.

1) For sufficiently large N and to an excellent degree of approximation, c grows *exponentially*, at least in the HE case. The solution I_n can thus be severely affected by roundoff and numerical integration errors. This is to be expected because (1) and (7) are Fredholm integral equations of the first kind, whose kernels $K(z)$ and $G(z)$ are smooth.
2) For large N, the HE system is much more ill-conditioned than the PE system. This is simply because $K(z)$ is smoother than $G(z)$—note the fifth power of R in (8).

[1]Attempting to solve DFG/PE for the *infinite-length* antenna via Fourier transformation does not lead to a solution because the Fourier inversion integral for $I(z)$ diverges exponentially. This statement can be shown as in [21], where it is shown for DFG/HE.

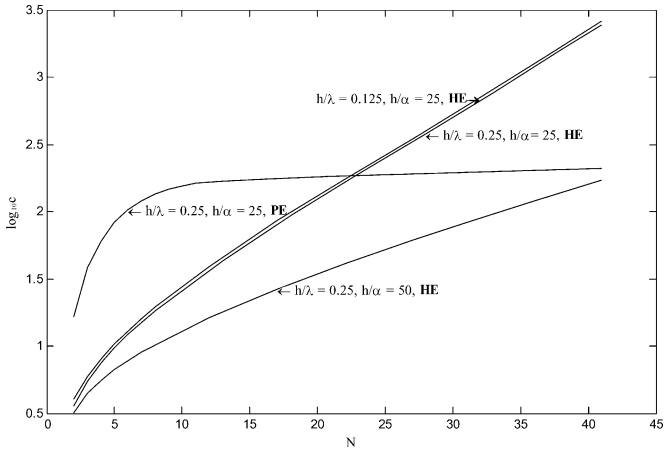

Fig. 4. Logarithm of 1-norm condition number c for the $(N+1) \times (N+1)$ system resulting from HE (three combinations of h/λ and a/λ) and the system resulting from PE.

3) Different values of h/λ and a/λ yield virtually the same c as long as h/a is fixed. And smaller values of the important parameter h/a imply much more ill-conditioning.

Because of the severity of matrix ill-conditioning, we took much care to ensure that the results in Figs. 1–3 are free of roundoff and numerical integration errors. To do this, we chose N not much larger than h/a, used double-precision arithmetic, and obtained identical results using various numerical integration and system solving routines. Thus, the oscillations in Figs. 1–3 cannot be attributed to roundoff or numerical integration errors; such oscillations would occur even with hypothetical "perfect" hardware and software (i.e., a computer with an infinite word length and error-free numerical integration routines).

V. Conclusion

In this paper, we applied Galerkin's method with entire-domain, cosine basis functions to selected integral equations with the approximate kernel (the use of equations of this type remains widespread) and observed oscillations near the endpoints ($z = \pm h$) and/or near the driving point ($z = 0$) of the wire antenna. We also examined the separate—but very important—effects of roundoff. The present paper supplements [11] and [21], in which subdomain basis functions were considered. In the subdomain case, oscillations occur in the "cells" adjacent to $z = \pm h$ and/or $z = 0$ [11], [21]. Thus, the present oscillatory behavior resembles that occurring with subdomain basis functions. In the present case, however, there are no adjacent cells, so we had not expected this similarity beforehand. In any case, the undesirable behavior that emerges from our figures for $I(z)/V$ (Figs. 1 and 3) and I_n/V (Fig. 2) is clear and instantly recognizable.

Acknowledgment

The authors would like to thank I. Tsimpiris and P. J. Papakanellos for useful discussions.

References

[1] B. J. Strait and A. T. Adams, "Analysis and design of wire antennas with applications to EMC," *IEEE Trans. Electromagn. Compat.*, vol. EMC-12, no. 2, pp. 45–54, May 1970.
[2] E. L. Bock, "Comments on 'analysis and design of wire antennas with application to EMC'," *IEEE Trans. Electromagn. Compat.*, vol. EMC-13, no. 1, pp. 22–24, Feb. 1971.

[3] G. Miano, L. Verolino, and V. G. Vaccaro, "A hybrid procedure to solve Hallén's problem," *IEEE Trans. Electromagn. Compat.*, vol. 38, no. 3, pp. 495–498, Aug. 1996.
[4] F. M. Tesche, M. V. Ianoz, and T. Karlsson, *EMC Analysis Methods and Computational Models*. New York, Wiley, 1997, ch. 4.
[5] B. Archambeault, O. M. Ramahi, and C. Brench, *EMI/EMC Computational Modeling Handbook*. Norwell, MA: Kluwer, 1998, ch. 4, 7.
[6] L. K. Warne and K. C. Chen, "Slot apertures having depth and losses described by local transmission line theory," *IEEE Trans. Electromagn. Compat.*, vol. 32, no. 3, pp. 185–196, Aug. 1990.
[7] D. Poljak, C. Y. Tham, and A. McCowen, "Transient response of nonlinearly loaded wires in a two media configuration," *IEEE Trans. Electromagn. Compat.*, vol. 46, no. 1, pp. 121–125, Feb. 2004.
[8] D. Poljak and V. Doric, "Time-domain modeling of electromagnetic field coupling to finite-length wires embedded in a dielectric half-space," *IEEE Trans. Electromagn. Compat.*, vol. 47, no. 2, pp. 247–253, May 2005.
[9] F. Gronwald, "Calculation of mutual antenna coupling within rectangular enclosures," *IEEE Trans. Electromagn. Compat.*, vol. 47, no. 4, pp. 1021–1025, Nov. 2005.
[10] C. A. Balanis, *Antenna Theory: Analysis and Design*, 3rd ed. New York: Wiley, 2005, sec. 8.3, 8.5.2.
[11] G. Fikioris, J. Lionas, and C. G. Lioutas, "The use of the frill generator in thin-wire integral equations," *IEEE Trans. Antennas Propag.*, vol. 51, no. 8, pp. 1847–1854, Aug. 2003.
[12] P. J. Davies, D. B. Duncan, and S. A. Funken, "Accurate and efficient algorithms for frequency domain scattering from thin wire," *J. Comput. Phys.*, vol. 168, pp. 155–183, 2001.
[13] D. H. Werner, "A method of moments approach for the efficient and accurate modeling of moderately thick cylindrical wire antennas," *IEEE Trans. Antennas Propag.*, vol. 46, no. 3, pp. 373–382, Mar. 1998.
[14] G. Fikioris, "An application of convergence acceleration methods," *IEEE Trans. Antennas Propag.*, vol. 47, no. 12, pp. 1758–1760, Dec. 1999.
[15] W. L. Stutzman and G. A. Thiele, *Antenna Theory and Design*. New York: Wiley, 1998.
[16] *NEC-WIN PRO User's Manual*, Antenna Analysis Software Version 1.1, Nittany Scientific, Inc., Hollister, CA, 1997.
[17] B. P. Rynne, "On the well-posedness of Pocklington's equation for a straight wire antenna and convergence of numerical solutions," *J. Electromagn. Waves Appl.*, vol. 14, pp. 1489–1503, 2000.
[18] M. C. van Beurden and A. G. Tijhuis, "Analysis and regularization of the thin-wire integral equation with reduced kernel," *IEEE Trans. Antennas Propag.*, vol. 55, no. 1, pp. 120–129, Jan. 2007.
[19] T. T. Wu, "Introduction to linear antennas," in *Antenna Theory, Part I*, R. E. Collin and F. J. Zucker, Eds. New York: McGraw-Hill, 1969, ch. 8, pp. 312–313.
[20] S. A. Schelkunoff, *Advanced Antenna Theory*. New York: Wiley, 1952, pp. 149–150.
[21] G. Fikioris and T. T. Wu, "On the application of numerical methods to Hallén's equation," *IEEE Trans. Antennas Propag.*, vol. 49, no. 3, pp. 383–392, Mar. 2001.
[22] G. Fikioris and A. Michalopoulou, "On the use of entire-domain basis functions in Hallen's integral equation with the approximate kernel," in *Proc. Mediterranean Microw. Symp. (MMS 2006)*, Genoa, Italy, Sep. 19–21, pp. 64–67.

Modeling Radiated Emissions Due to Power Bus Noise From Circuit Boards With Attached Cables

Haixin Ke, K. Morishita, Todd Hubing, N. Kobayashi, and T. Harada

***Abstract*—A two-step technique for modeling the radiation from circuit boards with attached cables is developed and applied to various board–cable structures. The technique divides a complex source geometry into two components. One component consists of differential-mode sources and the pieces of the structure that contribute to the differential-mode radiation. The other component consists of common-mode sources at cable attachment points and the parts of the structure that play a role in the radiation due to common-mode cable currents. The two component geometries are much easier to model than the complete structure. This modeling approach also provides the modeler with insight regarding the design parameters that most influence one type of radiation or the other.**

***Index Terms*—Balance, common-mode current, power bus noise, radiated emissions.**

I. Introduction

Printed circuit boards (PCBs) often have copper power and return (or *ground*) planes, and the return planes are usually connected to metallic objects such as cables or enclosures. For these types of structures, noise voltages between the power and return planes may induce significant common-mode currents on the attached metallic objects resulting in unacceptable radiated emissions. Although the *sources* of noise are normally on the board, the *antennas* are often the larger attached objects [1], [2]. It is often desirable to model the electromagnetic coupling between the noise on the board and the attached objects; however, this kind of modeling can present a significant challenge for full-wave numerical modeling techniques due to the small dimension of the board thickness and the relatively large dimensions of the attached cables and chassis.

One technique for simplifying this type of simulation [3] employs the equivalence theorem and replaces the plane pair with a magnetic current around the edges of the board. This technique works well for calculating the differential-mode radiation directly from the plane pair, but it is not an efficient method for determining the common-mode voltages that drive attached cables and enclosures.

Since it is the common-mode currents induced on the cables that are the primary concern, it can be advantageous to isolate the differential-mode sources and focus the modeling on just those aspects of the configuration that contribute to the common-mode currents. Techniques that use this approach are described in [4] and [5].

Recently, a two-step modeling technique was proposed that derives two simpler structures from the original PCB with cable/chassis attachments [6]. The first structure consists of the board's power and return planes with the attached cables and chassis removed. The second structure includes the cables and chassis, but eliminates the power plane and the dielectric substrate. The first structure is modeled to calculate the differential-mode voltage distribution between the power and return planes. The differential-mode voltages at discontinuities in the plane pair are then converted to equivalent sources and applied to the second

Manuscript received September 25, 2008; revised November 3, 2008. First published March 16, 2009; current version published May 15, 2009.

H. Ke and T. Hubing are with Clemson University, Clemson, SC 29634 USA (e-mail: hxkeucl@clemson.edu; hubing@clemson.edu).

K. Morishita, N. Kobayashi, and T. Harada are with NEC Corporation, Sagamihara 229-1198, Japan.

Color versions of one or more of the figures in this paper are available online at http://ieeexplore.ieee.org.

Digital Object Identifier 10.1109/TEMC.2008.2010947